minerals

MDPI

Article

Meso–Cenozoic Exhumation in the South Qinling Shan (Central China) Recorded by Detrital Apatite Fission-Track Dating of Modern River Sediments

Xu Lin [1,*], Jing Liu-Zeng [2], Lin Wu [3], Soares Jose Cleber [4], Dongliang Liu [5], Jingen Dai [6], Chengwei Hu [7], Xiaokang Chen [7], Lingling Li [7] and Liyu Zhang [7]

1 College of Civil Engineering and Architecture, China Three Gorges University, Yichang 443002, China
2 Institute of Surface-Earth System Science, Tianjin University, Tianjin 300072, China; liu_zeng@tju.edu.cn
3 State Key Laboratory of Lithospheric Evolution, Institute of Geology and Geophysics, Chinese Academy of Sciences, Bejing 100029, China; wulin08@mail.iggcas.ac.cn
4 ChronusCamp Research-Thermochronology Analysis Ltd., Itapira 13974-160, SP, Brazil; chronuscamp@gmail.com
5 Key Laboratory of Deep-Earth Dynamics of Ministry of Natural Resources, Institute of Geology, Chinese Academy of Geological Sciences, Beijing 100037, China; pillar131@163.com
6 State Key Laboratory of Biogeology and Environmental Geology, School of Earth Sciences and Resources, Research Center for Tibetan Plateau Geology, China University of Geosciences, Beijing 100083, China; daijingen@cugb.edu.cn
7 Key Laboratory of Geological Hazards on Three Gorges Reservoir Area, Ministry of Education, China Three Gorges University, Yichang 443002, China; z15684190512@163.com (C.H.); chenxiaokang555@163.com (X.C.); li0728100@163.com (L.L.); 13547685311@163.com (L.Z.)
* Correspondence: hanwuji-life@163.com

Abstract: The Qinling Shan is located between the North China Craton and the South China Block. Not only is investigating the exhumation process of the Qinling Shan beneficial for comprehending the tectonic collision history of mainland China but also for enhancing our understanding of the development of the Yellow and Yangtze Rivers. Previous studies have predominantly focused on bedrock analysis in the Qinling Shan. However, modern fluvial detrital samples offer a more extensive range of thermal history information. Therefore, we gathered modern fluvial debris samples from the Hanjiang River, which is the largest river in the South Qinling Shan. Subsequently, we conducted apatite fission-track analysis using the laser ablation inductively coupled plasma mass spectrometry (LA-ICP-MS) method. A total of 214 valid track ages were obtained, with an age distribution ranging from 9.5 to 334.0 Ma. The Density Plotter software was employed to decompose the data and generate four prominent age peaks: 185, 103, 69, 35, and 12 Ma. The exhumation events of the Early Jurassic (185 Ma) and Cretaceous (103–69 Ma) in the Southern Qinling Shan were strongly influenced by the collision between the South China Block and the North China Craton, as well as the subduction of the West Pacific Plate, respectively. The far-field effect of the collision between the Indian Plate and the southern Asian continent influenced the exhumation of the South Qinling Shan during the Late Eocene (35 Ma) and Middle Miocene (12 Ma), respectively. In conjunction with the reported findings, we comprehensively analyzed the geological implications of the Mesozoic and Cenozoic exhumations of the Qinling Shan. The Qinling Shan emerged as a watershed between the Ordos and Sichuan Basins in the early Mesozoic and Cenozoic, respectively. However, the exhumation and expansion of the Tibetan Plateau has forced the Yangtze River to flow eastward, resulting in its encounter with the South Qinling Shan in the late Cenozoic. The exhumation of the Qinling Shan has resulted in fault depression in the southern Ordos Basin. This geological process has also contributed to the widespread arid climatic conditions in the basin. During the Miocene, the Yellow River experienced limited connectivity due to a combination of structural and climatic factors. As a result, the Qinling Shan served as an obstacle, dividing the connected southern Yangtze River from the northern segment of the Yellow River during the late Cenozoic era.

Keywords: Qinling Shan; detrital apatite; fission track; Hanjiang River; Yangtze River; Yellow River

Citation: Lin, X.; Liu-Zeng, J.; Wu, L.; Cleber, S.J.; Liu, D.; Dai, J.; Hu, C.; Chen, X.; Li, L.; Zhang, L. Meso–Cenozoic Exhumation in the South Qinling Shan (Central China) Recorded by Detrital Apatite Fission-Track Dating of Modern River Sediments. *Minerals* **2023**, *13*, 1314. https://doi.org/10.3390/min13101314

Academic Editor: Manuel Francisco Pereira

Received: 19 September 2023
Revised: 8 October 2023
Accepted: 9 October 2023
Published: 11 October 2023

1. Introduction

Linear orogenic belts are geological regions where mountain ranges are formed as a result of tectonic plate collisions [1]. The immense forces generated by the collision cause the lithosphere, the rigid outer layer of the Earth, to fold, fault, and exhume, leading to the formation of linear orogenic belts [2]. Examples of linear orogenic belts include the Alps in Europe, the Appalachians in North America, the Andes in South America, and the Tian Shan and Qinling Shan ("Shan" is Chinese for "mountain") in Asia (Figure 1). These belts provide crucial information about the tectonic history and processes of the Earth [2,3]. Geologically, the Qinling Shan act as a major boundary between the North China Craton and the South China Block (Figure 1). Geographically, the Qinling Shan acts as a natural barrier, separating the humid southern regions of China from the drier areas in the northwest [4]. Additionally, the Qinling Shan serves as a geomorphic barrier by acting as a watershed, thus playing a significant role in the development of the Yangtze and Yellow Rivers, which are the two largest rivers in China [5]. Therefore, studying the process of exhumation in the Qinling orogenic belt is of the utmost importance in order to obtain a thorough understanding of the tectonic, landform, and large river evolution of Central China.

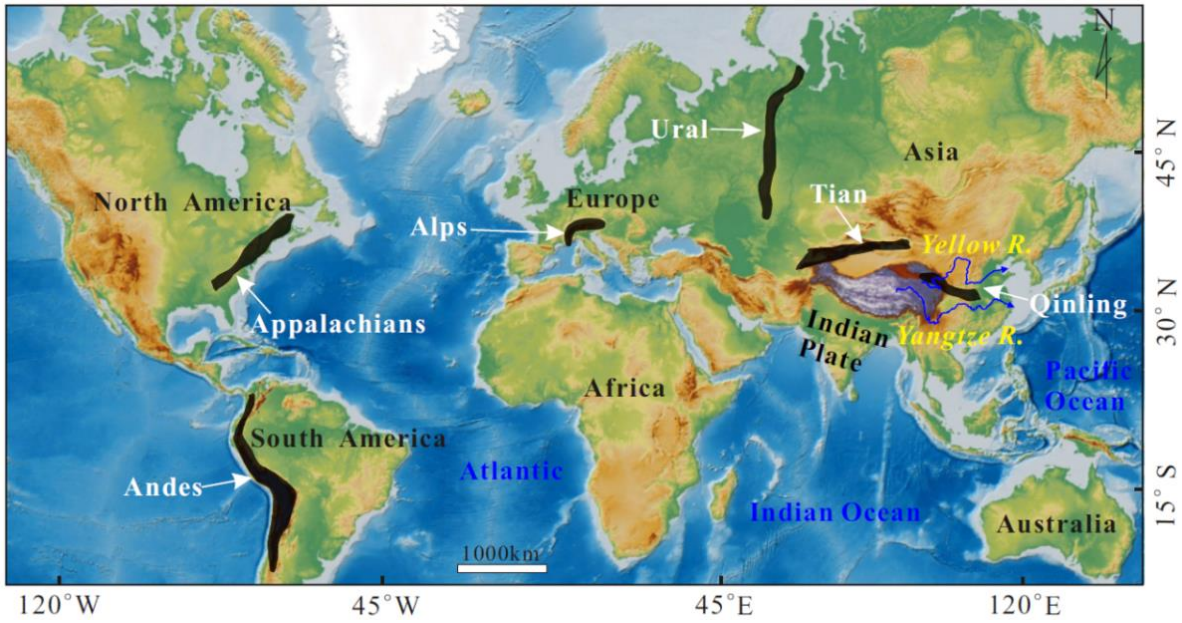

Figure 1. A map illustrating the major linear orogenic belts of the world [1]. The Qinling orogenic belt serves as the watershed between the Yellow and the Yangtze Rivers, two major large rivers in China.

Low-temperature thermochronology, such as apatite fission track (closer temperature 60–120 °C), has emerged as a popular method for investigating the exhumation of the Qinling orogenic belt [6–8]. However, most research in this field has primarily focused on the inner bedrock of the orogenic belt. The response of the bedrock in different parts of the same orogenic belt to tectonic exhumation during the same period is not synchronized [9–11]. This has led to notable differences in the timing of tectonic exhumation in the Qinling Shan, including the Mesozoic [12], early Cenozoic [13], and late Cenozoic [14]. Moreover, some studies have suggested that the formation of the Qinling Shan as the watershed between the Yellow and the Yangtze Rivers may have begun during the Late Cretaceous (80–70 Ma) [15]. However, other studies propose that this geological event occurred during the Early Eocene (50–40 Ma) [16] and Late Miocene (12–10 Ma) [17]. The exact timing of when the Qinling Shan became the watershed between the Yangtze and Yellow Rivers is still controversial (Figure 2a). Therefore, the fundamental solution to the above dispute lies in determining the exhumation time of the Qinling Shan. The low-temperature thermochronological age

of clastic sediments from rivers that flow in linear orogenic belts can provide more detailed information about the exhumation history of the orogenic belt [18–21]. This method has been extensively employed in the investigation of exhumation processes in linear orogenic belts, particularly the Alps in Europe [22–24], the Andes in South America [25], and the Tian Shan in Asia [26,27]. While conducting a modern fluvial apatite fission-track analysis on the tributaries of the Hanjiang River, You et al. [28] primarily focused their study on the exhumation history of the Daba Shan, which is a branch of the Qinling Shan (Figure 2b). Therefore, a comprehensive analysis of the exhumation history of the Qinling Shan has not been provided. In this study, we performed an analysis on the apatite fission-track age of fluvial clastic sediments in the Hanjiang River as it flows from west to east through the South Qinling Shan. By integrating these findings with existing bedrock low-temperature thermochronology and sedimentology results, it was possible to systematically determine the timing of exhumation for the entire Qinling Shan. Not only does this contribute to our understanding of the formation mechanism of linear orogenic belts, but it also provides valuable insight into the formation times of large rivers in China.

2. Geological Setting

2.1. Qinling Shan

The Qinling Shan, spanning approximately 1500 km, is a prominent mountain range running in Central China from east to west (Figure 2a). The Luonan–Luanchuan fault demarcates the boundary between the North Qinling Shan and the North China Craton [29,30] (Figure 2b). The Shangdan suture zone acts as the dividing line between the North and South Qinling Shan. The Mianlue suture zone distinguishes the South Qinling Shan from the South China Block.

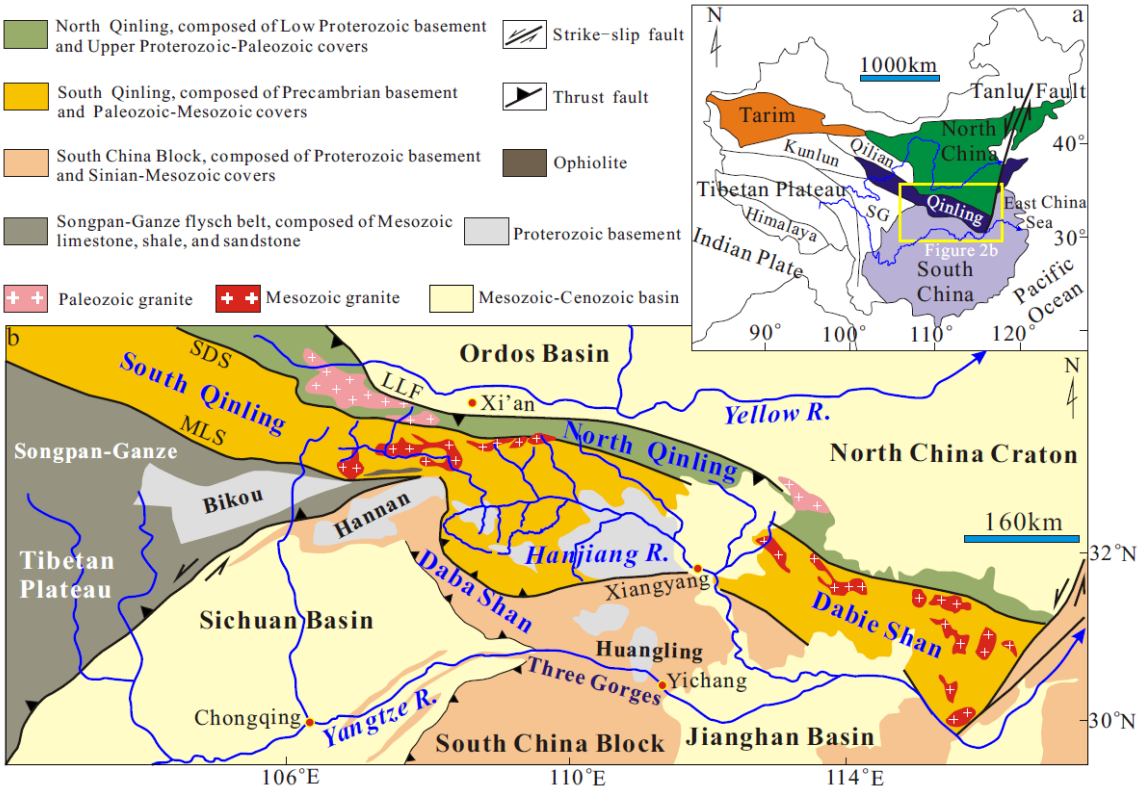

Figure 2. (**a**) The location map of the Qinling Shan; (**b**) The tectonic division map of the Qinling Shan (modified from Li et al. [30]). The Shangdan suture (SDS) zone is the boundary between the North and South Qinling Shan [29]. The Luonan–Luanchuan fault (LLF) delineates the boundary between the North Qinling Shan and the North China Craton. The South Qinling Shan and the South China Block are separated by the Mianlue suture (MLS) zone.

The geological history of the Qinling Shan is quite complex and spans several geological eras [31,32]. During the Mesozoic era, the Qinling orogenic belt underwent significant tectonic activity, characterized by the subduction of the Paleo-Tethys Ocean underneath the North China Craton [33] (Figure 3a). Eventually, the collision between the North China Craton and the South China Block during the Late Triassic to Early Jurassic period resulted in the closure of the Paleo-Tethys Ocean and the formation of the basic framework of the Qinling orogenic belt [31]. The mantle upwelling beneath the Qinling orogenic belt may have caused the crustal thickening and subsequent exhumation during the Late Cretaceous [34] (Figure 3b). The far-field effect of the collision between the Indian and the Asian Plates played a crucial role in shaping the early Cenozoic exhumation of the Qinling Shan [35] (Figure 3c). The late Cenozoic exhumation of the Qinling Shan is a significant geological event that shaped the topography of the region [36] (Figure 3d).

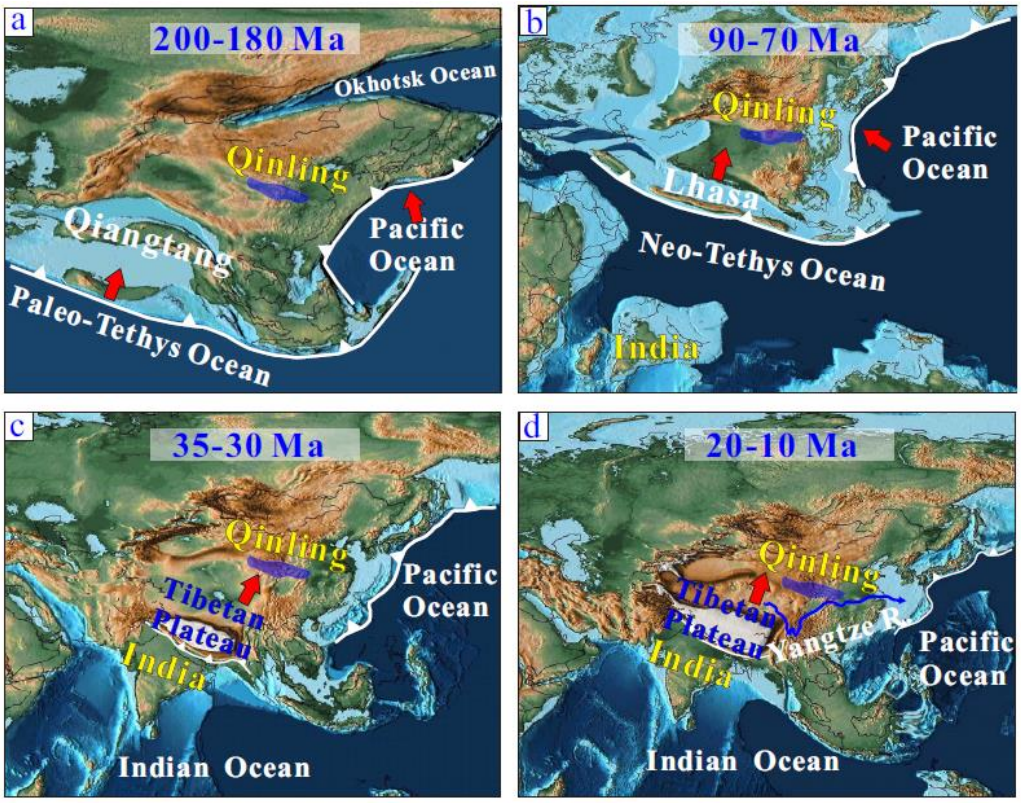

Figure 3. Maps depicting the Mesozoic and Cenozoic evolution of the Qinling Shan (http://www.earthbyte.org/paleomap{-}{-}-paleoatlas{-}{-}-for{-}{-}-gplates/, accessed on 10 August 2023): (**a**) the initial geological framework of the Qinling Shan was established during the early Mesozoic period when the South China Block collided with the North China Craton [31]; (**b**) in the Late Cretaceous, the Pacific Plate subducted beneath the Asian continent, resulting in the reactivation of the Qinling Shan [34]; (**c**) the far-field effects of the Eocene collision between the Indian Plate and the Asian continent influenced the Qinling Shan [35]; (**d**) in the late Cenozoic era, the Qinling Shan experienced further exhumation and became the watershed between the Yellow and the Yangtze Rivers [36]. The red arrows indicate the plate movement direction.

2.2. Sedimentary Basins

The sedimentary basins adjacent to the orogenic belt play a crucial role as repositories for the deposition and accumulation of sediments [37]. These sediments serve as valuable records, documenting the geological processes and changes taking place in the surrounding mountain range [38]. The sedimentary basins surrounding the Qinling Shan primarily consist of the Sichuan and Jianghan Basins in the northern region of the South China Block, as well as the Ordos Basin in the western regions of the North China Craton (Figure 2b). The

sediments deposited within these basins hold crucial information about the exhumation history of the Qinling Shan and the tectonic processes that have shaped the region over millions of years [35]. The Lower and Middle Triassic strata in the Sichuan (Figure 4a) and Jianghan Basins (Figure 4b) consist mainly of shallow marine deposits, whereas the Ordos Basin is dominated by continental strata [39–41] (Figure 4c). The Lower Jurassic strata in the Sichuan Basin are composed of sandy conglomerates and exhibit angular unconformity with the Upper Triassic strata [39]. In the Jianghan Basin, the Lower Jurassic strata directly contact the underlying strata and also contain conglomerate [40]. There is a parallel unconformity contact observed between the Lower Jurassic and the underlying Upper Triassic strata within the Ordos Basin [41]. However, there is a significant contrast in the Upper Cretaceous strata, particularly in the Sichuan and Ordos Basins, where these layers are noticeably lacking (Figure 4a,c). In contrast, the Upper Cretaceous strata in the Jianghan Basin are mainly composed of thick layers of conglomerate deposits. Additionally, an angular unconformity contact between the Paleogene and Neogene strata can be observed in both the Sichuan and Jianghan Basins. Moreover, the conglomerate layers are present in the late Neogene strata of the Ordos Basin [42].

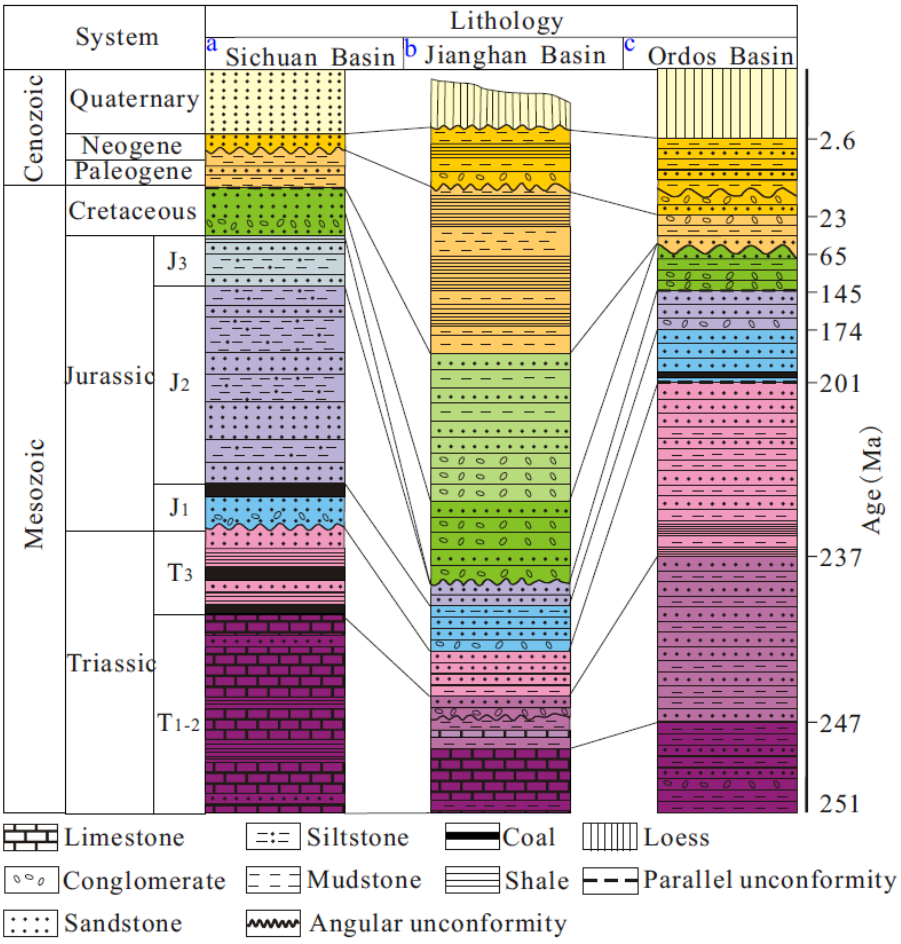

Figure 4. The main sedimentary basins surrounding the Qinling Shan include the (**a**) Sichuan Basin [39], (**b**) Jianghan Basin [40], and (**c**) Ordos Basin [41]. There is an angular unconformity observed between the Lower Jurassic and Upper Triassic formations in the Sichuan Basin [39]. The conglomerate layers have been identified in the Lower Jurassic strata of the Jianghan Basin [40]. A parallel unconformity between the Lower Jurassic and the underlying strata has been observed in the Ordos Basin [41]. The Upper Cretaceous strata are absent in the Sichuan and Ordos Basins, whereas thick conglomerates are present in the Jianghan Basin. In the Sichuan and Jianghan Basins, there is an angular unconformity between the Neogene and Paleogene strata. In the late Neogene strata of the Ordos Basin, conglomerates and angular unconformities can be observed [41,42].

2.3. Rivers

The emergence of large orogen belts can have a profound impact on the evolution of nearby large rivers, including significant changes in their course and even the occurrence of river capture [43–45]. Rivers play a vital role as channels for transporting material within orogenic belts and sedimentary basins. By analyzing the source of sediment in these basins and correlating it with the age of sedimentary layers, it is possible to reconstruct the river development sequence [5,37,43]. Consequently, the timing of the river formation can be used to constrain the tectonic evolution timeline of the associated orogenic belt.

As the largest tributary of the Yangtze River, the Hanjiang flows from west to east along the Late Cretaceous–Eocene fault basins of the South Qinling Shan [46]. It eventually merges with the Yangtze River in the Jianghan Basin, covering a total length of approximately 1577 km (Figure 5). The Yangtze River, stretching approximately 6300 km, is the largest river in China (Figure 2a). It originates in the southeastern edge of the Tibetan Plateau, goes through the northern region of the South China Plate, and eventually enters the East China Sea. In the past, the upper reaches of the Yangtze River used to flow into the South China Sea prior to the Early Eocene era [47–49]. However, its course has shifted to an eastern direction since the Miocene [50–53]. The Yellow River, with a length of 5464 km, is the second longest river in China. It originates in the northeastern part of the Tibetan Plateau and flows through the North China Craton before eventually emptying into the Bohai Sea (Figure 2a). The formation and development of the Yellow River took place over several stages during the Miocene and Pliocene periods [5,54–56]. By the Early Pleistocene, the entire basin of the Yellow River had become connected [57,58].

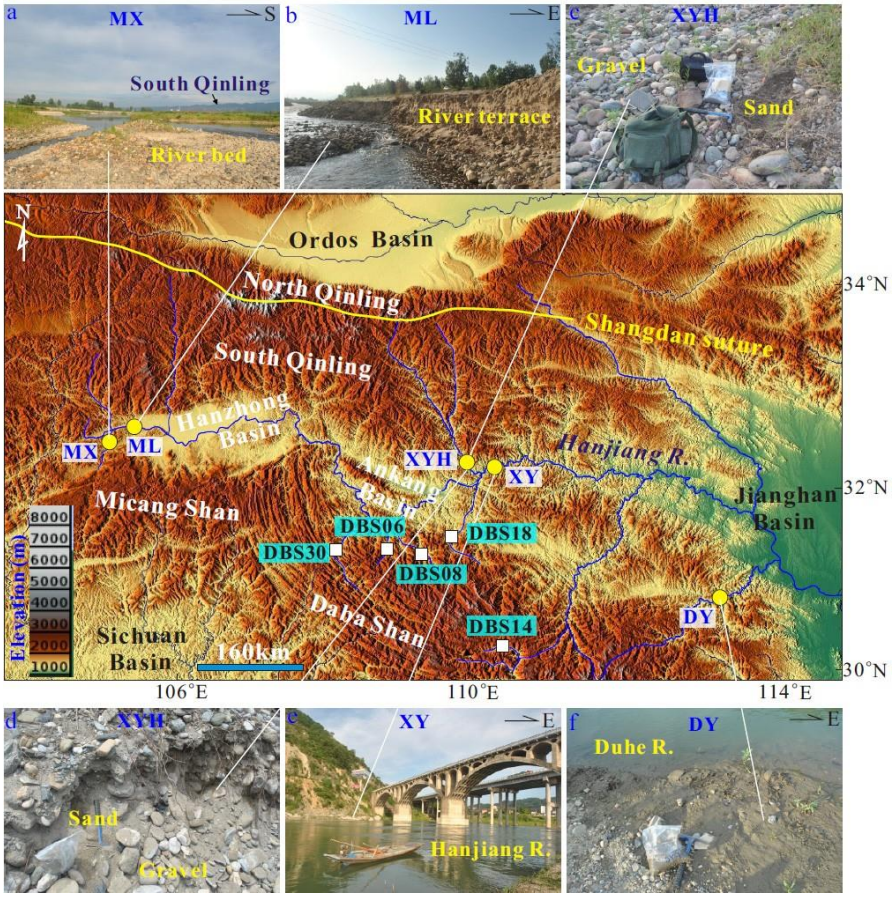

Figure 5. Map illustrating the geographical distribution of field sample locations (https://maps-for-free.com/, accessed on 15 August 2023). The yellow circles on the map indicate the distribution of the samples collected in the Hanjiang River Basin for the present study (**a**–**f**). The white boxes denote the sampled areas of Daba Shan (South Qinling) from the study conducted by You et al. [28].

3. Methods

We collected fluvial sand samples from different locations along the main stream and tributaries of the Hanjiang River (refer to Figure 5). Multiple sites were sampled for each sample to ensure that the collected sample provided the most representative information on low-temperature thermochronology in the basin. Sample MX was collected from a tributary of the Micang Shan, while sample ML was collected from the main stream of the Hanjiang River. Sample XYH came from a tributary at the southern piedmont of the South Qinling Shan, and sample XY was collected from the main stream of the Hanjiang River. Lastly, sample DY came from a tributary of Daba Shan. The selected sampling sites provide comprehensive coverage across the South Qinling Shan. The apatite mineral separation was performed using routine separation methods. This involved initial stages of jaw crushing and milling, which were followed by subsequent processes of sieving, washing, magnetic separation, and heavy liquid separation. These procedures were carried out at Hebei Langfang Chengxin Geology Co., Ltd. (Langfang, China), in China. Each sample was carefully handpicked under a microscope to ensure the selection of pure apatite grains suitable for fission-track analysis. The chosen grains were then mounted on Teflon and polished to expose their internal surfaces. The dating of all samples was conducted at the ChronusCamp Research-Thermochronology Laboratory facilities (Itapira, Brazil) in Brazil using laser ablation inductively coupled plasma mass spectrometry (LA-ICP-MS).

The apatite grains were etched in 5.5 M HNO_3 for 20 s at a temperature of 21 °C in order to enhance the visibility of the fission tracks [59]. An ultrathermostatic water batch was utilized to regulate the temperature during the etching procedure. The apatite fission tracks were calibrated using the Durango standard as the age sample [60]. The concentration of ^{238}U was determined using uranium standards (Dur-2 and MT-7) with a U variation of less than 1.5% [61]. The isotope concentration was determined using an Agilent 7800 ICP-MS (Santa Clara, CA, USA) coupled to a 193 Analyte Excite laser ablation system. A gas mixer (Squid) was connected to the laser ablation system for better homogenization of the isotope mixture. Isotope data were acquired with spot size for the laser ablation chosen to cover the largest area of apatite grains possible where the fission tracks were analyzed [60], a laser energy of approximately 5 J/cm^2 with a repetition rate of 5 Hz, and shutter delay of 30 s. Finally, NIST SRM 610 was analyzed along with the age and uranium standards to assess the performance of LA-ICP-MS during the analysis [61]. Spontaneous fission tracks were counted using a fully automated Leica DM6M microscope(Wetzlar, Germany) at a nominal magnification of 1000×, dry. Fission-track ages were determined using the calibration method described in the study by Hurford and Green [62]. The value of the Zeta calibration was determined by taking into account the age of Durango (31.44 ± 0.18 Ma) using $^{40}Ar/^{39}Ar$ dating as reported by McDowell et al. [63]. We used the Density Plotter software developed by Vermeesch [64] to form radial plots and kernel–density estimate curves for the apatite fission-track ages.

4. Results

A total of 214 detrital apatite grains (see Supplementary Materials Table S1) collected from the main stream and tributaries of the Hanjiang River were analyzed (Figure 6; Table 1). The sample MX exhibited three distinct fission-track age peaks, which were found to be 32.6 ± 2.9, 73.7 ± 3.0, and 204.0 ± 31.0 Ma (Figure 6a). The age peaks of the sample ML were 17.0 ± 12.0, 82.8 ± 4.5, and 193.0 ± 39.0 Ma (Figure 6b). The sample XYH included three peak ages: 17.6 ± 2.3, 65.4 ± 3.0, and 157.0 ± 17.0 Ma (Figure 6c). The sample XY presented two distinct peaks: 44.1 ± 7.8 and 104.9 ± 87.8 Ma (Figure 6d). The sample DY exhibited two distinct age peaks: 19.0 ± 15.0 and 109.0 ± 24.0 Ma (Figure 6e). Finally, we assembled all the fluvial detrital samples for age estimation and identified four age peaks: 11.8 ± 1.8, 34.6 ± 3.4, 69.3 ± 4.1, 103.0 ± 14.0, and 185.0 ± 19.0 Ma (Figure 6f). You et al. [28] conducted a fission-track age analysis of detrital apatite collected from rivers in the Daba Shan (Figure 5). One notable finding from their study is the absence of Miocene and Early Jurassic age peaks in the analyzed samples. This could be attributed to the fact

that their samples were predominantly collected from small rivers, which provided more localized low-temperature thermochronological information. However, the remaining age peak components are concentrated in the Late Eocene (34.8 ± 7.6 Ma), Cretaceous (116.0 ± 12.0–69.0 ± 8.9 Ma), and Late Jurassic (152.0 ± 34.0 Ma), which are in line with the findings of our analysis. Please consult Table 1 for more specific details.

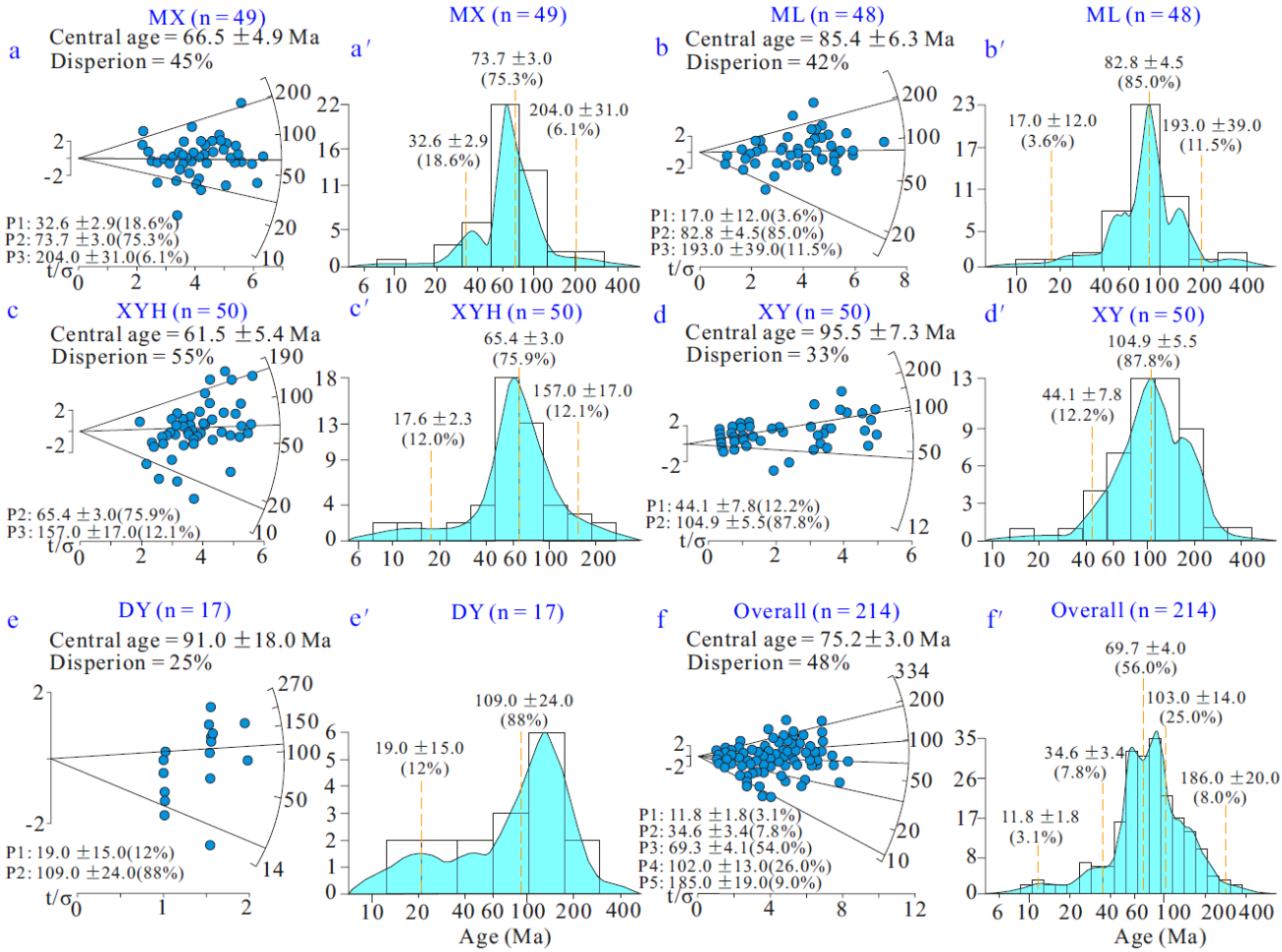

Figure 6. Detrital apatite fission-track results were obtained for modern samples collected from the Hanjiang River: (**a**–**f**) depict the single-grain age data in radial plots on the left and the grain-age distribution in terms of probability plots and kernel density estimates on the right (**a′**–**f′**). Both plots were generated using Density Plotter (Vermeesch [64]). As shown in (**f**,**f′**), the ages of individual grains from various rivers were combined.

Table 1. The detrital apatite fission-track results obtained from samples collected from the Hanjiang River drainage in this study are compared with previously published data.

Sample	GPS	N	P1 Ma	P2 Ma	P3 Ma	P4 Ma	P5 Ma	Data Source
MX	106°43′18″ 33°08′51″	49		32.6 ± 2.9 (18.6%)	73.7 ± 3.0 (75.3%)		204.0 ± 31.0 (6.1%)	This study
ML	106°44′29″ 33°08′49″	48	17.0 ± 12.0 (3.6%)		82.8 ± 4.5 (85.0%)		193.0 ± 39.0 (11.5%)	
XYH	109°20′07″ 32°49′18″	50	17.6 ± 2.3 (12%)		65.4 ± 3.0 (75.9%)	157.0 ± 17.0 (12.1%)		
XY	109°24′00″ 32°50′8″	50		44.1 ± 7.8 (12.2%)	104.9 ± 87.8 (87.8%)			
DY	110°33′43″ 32°41′10″	17	19.0 ± 15.0 (12%)		109.0 ± 24.0 (88%)			

Table 1. *Cont.*

Sample	GPS	N	P1 Ma	P2 Ma	P3 Ma	P4 Ma	P5 Ma	Data Source
DBS06	32°25.13′ 108°39.71′	19			116.0 ± 12.0 (100%)			
DBS08	32°25.55′ 108°52.25′	67		36.8 ± 7.6 (6.3%)	85.9 ± 6.1 (73%)	152.0 ± 34.0 (21%)		You et al. [28]
DBS14	31°57.65′ 109°31.45′	53			69.0 ± 8.9 (72%)	140.0 ± 29.0 (28%)		
DBS18	32°30.36′ 109°09.47′	22			102.6 ± 7.1 (100%)			
DBS30	32°1.46′ 108°35.87′	43			101.8 ± 6.7 (100%)			

5. Discussion

To improve the statistical reliability of the fission-track ages derived from identical fluvial apatite grains, researchers typically aggregate all of the samples that have been analyzed for age decomposition. Therefore, we focused on five age peaks decomposed together in all of the samples from the Hanjiang River Basin: 185, 103, 69, 35, and 12 Ma. The peak age of these decomposed apatite fission tracks is younger than the ages of the Precambrian and Paleoproterozoic basement rocks in the basin (Figure 2b). Therefore, these age peaks may indicate exhumation events in the South Qinling Shan since the early Mesozoic era.

5.1. The Mesozoic Exhumation

Our detrital apatite fission-track data indicate that the exhumation of the South Qinling Shan commenced around 185 Ma (Figure 7(1)). This age corresponds to the convergence of the North China Craton and the South China Block during the Late Triassic–Early Jurassic [29,31,65–67]. According to Li et al. [30] and Yang et al. [68], the ages determined using the ^{40}Ar-^{39}Ar and zircon fission-track dating methods demonstrate that the rapid exhumation of the Southern Qinling Shan occurred simultaneously around 180 Ma (Figure 7(2,3)). There is an angular unconformity observed between the Lower Jurassic and the underlying Upper Triassic strata in the northern Sichuan Basin [39] (Figure 4a), suggesting the occurrence of regional tectonic events (Figure 7(4)). The gravel and sandstone found in the northern Jianghan Basin document the unroofing history of the South Qinling Shan during the Early Jurassic [40,69] (Figure 4b; Figure 7(5)). At the same time, previous studies have demonstrated the U-Pb provenance tracing results of detrital zircon, which indicate that the South Qinling Shan served as a stable provenance area in the northern Sichuan Basin during the Early Jurassic [39,70,71] (Figure 7(6)). The unannealed zircon fission-track and zircon (U-Th)/He ages obtained from these formations in the northern Sichuan Basin indicate that the exhumation of the South Qinling Shan occurred between 196 and 180 Ma [66,72] (Figure 7(7,8)). The denuded North Qinling Shan emerged as a crucial source area in the southern Ordos Basin [41,73] (Figure 7(9)). The apatite fission-track and (U-Th)/He analyses of the sedimentary layers from the southern Ordos Basin indicate that rapid exhumation occurred in the North Qinling Shan at 180–165 Ma [74,75] (Figure 7(10,11)). Therefore, the Qinling orogenic belt underwent extensive exhumation during the Early Jurassic period, leading to the accumulation of a significant amount of clastic sediment in the adjacent sedimentary basins.

Our sample data indicate that there was another significant period of intense exhumation in the South Qinling Shan during the Late Cretaceous period around 103–69 Ma (Figure 7(12)). This event shows similarities to the process of exhumation of fluvial detrital apatite fission tracks in the Daba Shan (86–69 Ma), as documented by You et al. [28] (Figure 7(13)). It is also extensively observed in the bedrock of the South Qinling Shan. For instance, previous studies have utilized apatite and zircon fission-track ages to document the fast exhumation of the South Qinling Shan during 90–60 Ma [7,8,68,76–78] (Figure 7(14,15)). Detrital apatite fission-track and (U-Th)/He ages of zircon in the Mesozoic strata in the northern Sichuan Basin provide evidence for exhumation in the South Qinling

Shan occurring between 80 and 70 Ma [79,80] (Figure 7(16,17)). The analysis of detrital apatite fission-track ages on the Mesozoic strata in the northern Jianghan Basin, conducted by Peng et al. [81], indicates that the South Qinling Shan underwent exhumation between 100 and 82 Ma (Figure 7(18)). Similarly, the detrital apatite fission-track and (U-Th)/He age data collected from the Mesozoic sandstones in the southern Ordos Basin suggest that the North Qinling Shan experienced exhumation around 110 Ma [74] (Figure 7(19)). Integrated apatite fission-track and apatite (U-Th)/He dating suggest that a phase of exhumation occurred in the North Qinling Shan during the Late Cretaceous (100–73 Ma [82]; Figure 7(20)). The detrital zircon U-Pb age provenance tracing and paleo-flow recovery results suggest that the Qinling Shan served as the source region of sedimentation for the Late Cretaceous in the Sichuan Basin [70] (Figure 7(21)), Jianghan Basin [83] (Figure 7(22)), and Ordos Basin [84] (Figure 7(23)). The presence of thick conglomerate within the Upper Cretaceous strata in the northern Jianghan Basin and the southern Ordos Basin suggests a period of an unroofing event within the South Qinling Shan during this time [40,41] (Figure 7(24)). The Qinling orogenic belt experienced a NE–NW extrusion during the Late Cretaceous, as reported by Enkelmann et al. [7]. This suggests a possible correlation between this tectonic exhumation event and the subduction of the Pacific plate beneath Eurasia [8,85–87].

5.2. Cenozoic Exhumation

Our fluvial detrital apatite fission-track age suggests that the exhumation of the South Qinling Shan occurred in 35 Ma during the early Cenozoic period (Figure 7(25)). You et al. [28] reported that the concentration of peak age fluoclastic apatite fission tracks in the Daba Shan during the early Cenozoic occurred predominantly at 37 Ma (Figure 7(26)). The zircon and apatite fission-track ages near the source of the Hanjiang River constrain the timing of exhumation to 40 Ma [17] (Figure 7(27)). The bedrock apatite fission-track and (U-Th)/He age confirm the exhumation of the western South Qinling Shan at 38–35 Ma [88–90] (Figure 7(28)). This result is consistent with the findings from clastic apatite fission-tracks and provenance tracing in nearby sedimentary basins, which indicate exhumation occurred between 34 and 30 Ma [91,92] (Figure 7(29,30)). The eastern parts of the South Qinling Shan also underwent rapid exhumation during the Late Eocene (35–30 Ma; Figure 7(31)), as described by Richardson et al. [16] and Ge et al. [93]. During the Eocene period, the relationship between the South Qinling Shan and Jianghan Basin was further strengthened through basin–mountain coupling [94,95] (Figure 7(32)). The bedrock apatite fission-track age in the vertical section is predominantly focused on 35 Ma, suggesting that rapid exhumation occurred in the North Qinling Shan during the Late Eocene [13,96] (Figure 7(33)). A notable fault depression occurred in the southern Ordos Basin during the Eocene, as documented by Meng and Zhang [31]. Lu et al. [97] further highlighted that this depression received detrital sediments from the North Qinling Shan (Figure 7(34)). Therefore, Late Eocene exhumation events were widespread in the Qinling Shan. The Indian plate was undergoing subduction beneath southern Asia during the Eocene [98,99]. Consequently, we can infer that the Qinling Shan region experienced rapid exhumation, which can be attributed to the northward expansion of the Tibetan Plateau during this period.

Another exhumation event occurred in the South Qinling during the Middle Miocene (12 Ma; Figure 7(35)). The findings from the low-temperature thermochronology analysis on the bedrock suggest that exhumation rates in the South Qinling region experienced a substantial rise around 12–8 Ma [7,14,17,76,91] (Figure 7(36)). The sedimentary strata in the northern Sichuan Basin underwent significant exhumation [79,100] (Figure 7(37)), with an angular unconformity observed at 15–10 Ma [39] (Figure 7(38)). Rapid exhumation in the North Qinling Shan occurred around 10 Ma, as documented by several studies [7,13] (Figure 7(39)). This exhumation led to the development of an angular unconformity and the deposition of conglomerate in the southern Ordos Basin [42] (Figure 7(40)). During the late Cenozoic, the Tibetan Plateau underwent notable exhumation as a single entity [97,101–104]. As a consequence, its eastern side experienced displacement towards the north and south, leading to intensive exhumation in the peripheral regions adjoining

the plateau around 12–10 Ma. Therefore, the outward expansion of the Tibetan Plateau during the Cenozoic era played a crucial part in the exhumation process of the Qinling orogenic belt.

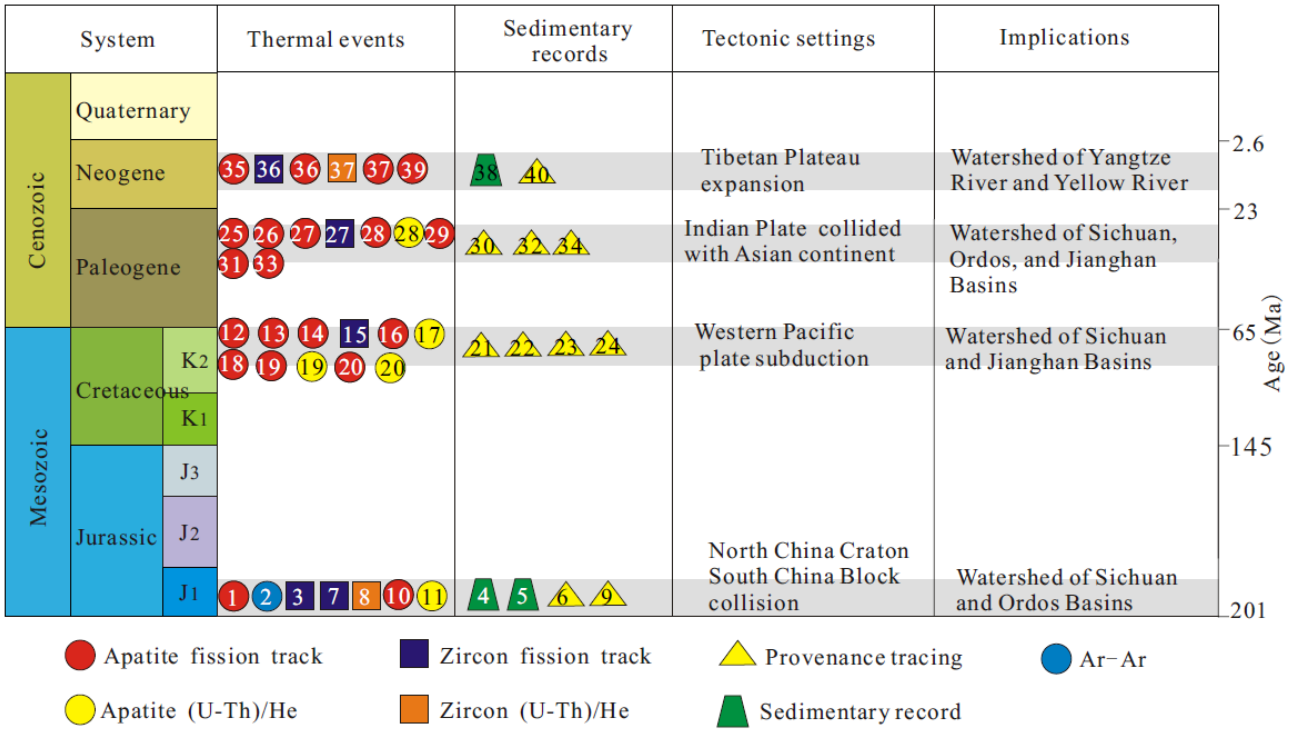

Figure 7. A summary map of Mesozoic and Cenozoic thermal events, sedimentary records, tectonic settings, and geological significance in the Qinling Orogenic Belt: (1) this study; (2) [30]; (3) [68]; (4) [39]; (5) [40,67]; (6) [39,70,71]; (7) [65]; (8) [72]; (9) [41,73]; (10) [74]; (11) [75]; (12) This study; (13) [28]; (14) [7,8,76–78]; (15) [67]; (16) [79]; (17) [80]; (18) [81]; (19) [74]; (20) [82]; (21) [70]; (22) [83]; (23) [84]; (24) [40,41]; (25) This study; (26) [28]; (27) [17]; (28) [88–90]; (29) [91]; (30) [92]; (31) [16,93]; (32) [94,95]; (33) [13,96]; (34) [97]; (35) This study; (36) [7,14,17,76,91]; (37) [81,100]; (38) [39]; (39) [7,13]; (40) [42].

5.3. Implications

The Mesozoic and Cenozoic exhumation of the Qinling orogenic belt holds great geological significance. This exhumation has played a crucial role in the tectonic evolution and geodynamic processes of the region.

During the Late Triassic and Early Jurassic, the collision between the South China Block and the North China Craton resulted in significant exhumation of the Qinling Shan [29,30,105–107]. Materials generated from the denudation of the Qinling Shan are carried by rivers and deposited into the Ordos Basin to the north and the Sichuan Basin to the south [70,105] (Figure 8a). Therefore, the Qinling Shan developed as a watershed between the northern Sichuan Basin and the southern Ordos Basin during the early Mesozoic period. The emergence of the Qinling Shan marked the completion of the main framework of mainland China in the early Mesozoic era.

Entering the Late Cretaceous, the eastern parts of East Asia experienced profound geological changes due to the subduction of the Western Pacific Plate [33,35,69,85]. At that time, a series of large-scale fault basins were formed in the South China Block, such as the Jianghan Basin [108]. The eastern parts of the South Qinling Shan served as the primary source area for the northern Jianghan Basin [40,83]. The Huangling anticline, situated in the South Qinling Shan, experienced a rapid process of exhumation during the Late Cretaceous, leading to the development of a regional watershed [83,109]. This exhumation led to the

formation of large rivers that flowed into the Jianghan Basin and Sichuan Basin on the east and west sides of the Huangling anticline, respectively [110,111]. The western parts of East Asia, however, were greatly influenced by the collision between the Lhasa Plate and the Asian continent, which led to the emergence of plateau landforms [112–117], as well as the formation of major rivers that flow into the Sichuan Basin [118–121]. Thus, the open southern Sichuan Basin developed into the primary site of sediment depocenter for a large river that originated in the eastern Tibetan Plateau and Qinling Shan (Figure 8b).

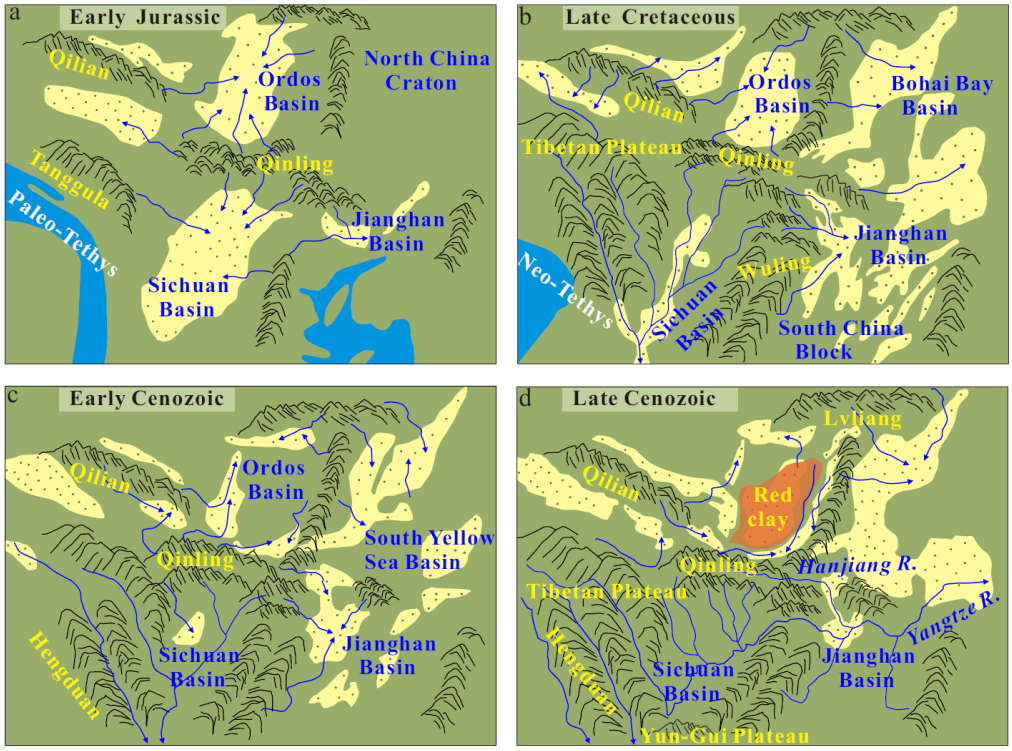

Figure 8. Geomorphic pattern around the Qinling orogenic belt in the Mesozoic and Cenozoic. (**a**) In the early Mesozoic era, the Qinling orogenic belt experienced exhumation due to the collision between the North China Craton and the South China Block [29,30]. This exhumation led to the development of the Qinling Shan, which served as the watershed between the Ordos Basin and the Sichuan Basin [105–107]. (**b**) In the late Mesozoic period, the subduction of the Western Pacific plate beneath the Asian continent led to the exhumation of the Qinling orogenic belt [7,8]. (**c**) The exhumation of the Qinling Shan during the early Cenozoic era was influenced by the distant effects of the collision between the Indian Plate and Asian continents [17]. (**d**) In the late Cenozoic era, the Tibetan Plateau underwent a northward and easterly expansion, which resulted in the exhumation of the Qinling Shan [7,17]. The Qinling Shan has acted as a natural boundary, separating the connected Yangtze River basin from the segmented Yellow River basin.

During the early Cenozoic era, a large river system developed from the southern piedmont of the Qinling Shan and extended southwards into the Sichuan Basin [44,47,119] (Figure 8c). This is primarily due to the limited occurrence of lateral extrusion on the Tibetan Plateau and the absence of significant exhumation in the Yunnan–Guizhou Plateau within the southern Sichuan Basin [122,123]. However, the formation of fault depression basins in the southern, northern, and western parts of the Ordos Basin was influenced by the outward expansion of the northeastern margin of the Tibetan Plateau [124,125]. These basins subsequently developed into localized sedimentary centers [126], which hindered the connectivity of the Yellow River [124]. During this period, the Jianghan Basin primarily experienced the deposition of salt lake sediments [127]. Additionally, the eastern parts of the South Qinling continued to serve as the main source area in the northern parts of the

Jianghan Basin [94]. The formation of the large river connecting the Sichuan Basin and the Jianghan Basin from west to east has not yet occurred during the Late Eocene [111].

The late Cenozoic was a period characterized by significant geological and geomorphological changes in the Qinling Shan and its surrounding regions [7]. Firstly, because of the continuous exhumation in the Qinling Shan and the Lvliang Shan, the two mountain ranges have become major geographical barriers for the transportation of eolian sediments in Northwest China [128–130] (Figure 8d). Therefore, extensive deposits of red clay have developed in the northern and western foothills of the Qinling Shan and the Lvliang Shan, respectively [131,132]. Secondly, the fault basins around the Ordos Plateau underwent significant development during the late Cenozoic, resulting in the formation of geomorphic obstacles that impeded the flow of the Yellow River [124,125]. Thirdly, the Yunnan–Guizhou Plateau experienced a strong exhumation during the late Cenozoic due to the outward expansion of the southeastern margin of the Tibetan Plateau [122,123]. This exhumation event led to the obstruction of the southward flow of a large river system originated in the Qinling Shan. In addition, it has been reported that during the late Cenozoic, the Jinshajiang River's course changed from a southward flow and started flowing eastward into the Sichuan Basin [133–136]. Detrital material originating from the eastern margin of the Tibetan Plateau was deposited in the Jianghan Basin during the Middle Miocene period, as shown by Yang et al. [137]. This finding suggests that the river connecting the Sichuan Basin and Jianghan Basin had reached a state of maturity during this period [17]. The Qinling orogenic belt underwent a transformation from a north–south division during the early Mesozoic to an west–east river divide in the late Cenozoic. However, the Yellow River flowed out of the Ordos Basin in a west-to-east direction during the early Pleistocene [5,57,58]. As a result, the emergence of the Yangtze River and the Yellow River flowing from west to east on the north and south sides of the Qinling Shan was not synchronized. In addition to the deep rift basin formed between the southern Ordos Basin and the North Qinling Shan [124], the late Miocene exhumation of the Qinling Shan resulted in climatic effects that contributed to the aridity of the Ordos Basin [130]. This aridity, in turn, became a significant barrier to the outflow of the Yellow River. Therefore, the exhumation of the Qinling Shan in the late Cenozoic era ultimately affected the spatial distribution of landscapes between the North China Craton and South China Block.

6. Conclusions

Based on the analysis of modern fluvial clastic apatite fission-track ages in the Hanjiang River, in combination with the published results of low-temperature thermochronology and sedimentology, we present information on the uplift of the South Qinling Shan since the Early Jurassic.

We identified five major exhumation events, with the Early Jurassic (185 Ma) exhumation primarily attributed to the collision between the North China Craton and the South China Block. The exhumation of the South Qinling Shan during the Cretaceous (103–69 Ma) was primarily driven by the subduction of the Western Pacific Plate beneath the Asian continent. During the early Cenozoic era, the Indian Plate collided with the southern margin of the Asian continent. This collision had a far-field effect, resulting in the exhumation of the South Qinling Shan during the Late Eocene (35 Ma). Furthermore, there was an expansion along the northeastern margin of the Tibetan Plateau, which led to significant exhumation of the South Qinling Shan during the Middle Miocene (12 Ma). Spatially, the exhumation of the South and the North Qinling Shan occurred concurrently during the Mesozoic and Cenozoic periods. As a result, the Qinling orogenic belt primarily served as the watershed for north–south flowing rivers in the Mesozoic and early Cenozoic, and as the boundary between the east–west flowing Yangtze and Yellow Rivers in the late Cenozoic.

Supplementary Materials: The following supporting information can be downloaded at: https://www.mdpi.com/article/10.3390/min13101314/s1, Table S1: Fission track results of detrital apatite in the Hanjiang River.

Author Contributions: Conceptualization, X.L. and J.L.-Z.; methodology, L.W. and S.J.C.; software, S.J.C.; validation, X.C., C.H., L.L. and L.Z.; formal analysis, C.H.; investigation, X.L.; resources, X.L.; data curation, X.L.; writing—original draft preparation, X.L.; writing—review and editing, J.L.-Z.; visualization, X.L.; supervision, D.L. and J.D.; project administration, X.L.; funding acquisition, X.L. and J.L.-Z. All authors have read and agreed to the published version of the manuscript.

Funding: This work was financially supported by the National Natural Science Foundation of China (Grants: 41972212 and 42030305), Open Foundation of Research Institute of Petroleum Exploration and Development, China National Petroleum Corporation (CNPC) (Grant: 2022-KFKT-36), and state of São Paulo Research Foundation (2011/21296-0 (PIPE-I) and 16/50500-8 (PIPE-II)).

Data Availability Statement: The data presented in this study are available on request from the corresponding author.

Acknowledgments: We thank Yu Xiang for his help with the field sample collection.

Conflicts of Interest: The authors declare no conflict of interest.

References

1. Dewey, J.F.; Bird, J.M. Mountain belts and the new global tectonics. *J. Geophys. Res. Earth Surf.* **1970**, *75*, 2625–2647. [CrossRef]
2. Dewey, J.F. Extensional collapse of orogens. *Tectonics* **1988**, *7*, 1123–1139. [CrossRef]
3. Jolivet, M.; Dominguez, S.; Charreau, J.; Chen, Y.; Li, Y.; Wang, Q. Mesozoic and Cenozoic tectonic history of the central Chinese Tian Shan: Reactivated tectonic structures and active deformation. *Tectonics* **2010**, *29*, 1–30. [CrossRef]
4. Dong, Y.; Shi, X.; Sun, S.; Sun, J.; Hui, B.; He, D.; Chong, F.; Yang, Z. Co-evolution of the Cenozoic tectonics, geomorphology, environment and ecosystem in the Qinling Mountains and adjacent areas, Central China. *Geosyst. Geoenviron.* **2022**, *1*, 100032. [CrossRef]
5. Lin, X.; Liu, J.; Liu, W.; Zhang, P.; Wang, B.; Liu, H. *Development and Evolution of Yellow River and Yangtze River*; Geological Publishing House: Beijing, China, 2023; pp. 1–181. (In Chinese with English Abstract)
6. Li, J.; Zhang, Y.; Dong, S.; Shi, W.; Li, H.L. Apatite fission track thermochronologic constraint on Late Mesozoic uplifting of the Fenghuangshan basement uplift. *Chin. J. Geol.* **2010**, *45*, 969–986. (In Chinese with English Abstract)
7. Enkelmann, E.; Ratschbacher, L.; Jonckheere, R.; Nestler, R.; Fleischer, M.; Gloaguen, R.; Ma, S. Cenozoic exhumation and deformation of northeastern Tibet and the Qinling: Is Tibetan lower crustal flow diverging around the Sichuan Basin? *Geol. Soc. Am. Bull.* **2006**, *118*, 651–671. [CrossRef]
8. Hu, S.; Raza, A.; Min, K.; Kohn, B.P.; Reiners, P.W.; Ketcham, R.A.; Wang, J.; Gleadow, A.J.W. Late Mesozoic and Cenozoic thermotectonic evolution along a transect from the north China craton through the Qinling orogen into the Yangtze craton, central China. *Tectonics* **2006**, *25*, 1–15. [CrossRef]
9. Burbank, D.W.; Leland, J.; Fielding, E.; Anderson, R.S.; Brozovic, N.; Reid, M.R.; Duncan, C. Bedrock incision, rock uplift and threshold hillslopes in the northwestern Himalayas. *Nature* **1996**, *379*, 505–510. [CrossRef]
10. Enkelmann, E.; Zeitler, P.K.; Pavlis, T.L.; Garver, J.I.; Ridgway, K.D. Intense localized rock uplift and erosion in the St Elias orogen of Alaska. *Nat. Geosci.* **2009**, *2*, 360–363. [CrossRef]
11. Lin, X.; Tian, Y.; Donelick, R.A.; Liu-Zeng, J.; Cleber, S.J.; Wu, Q.; Li, Z. Mesozoic and Cenozoic tectonics of the north-eastern edge of the Tibetan plateau: Evidence from modern river detrital apatite fission-track age constraints. *J. Asian Earth Sci.* **2019**, *170*, 84–95. [CrossRef]
12. Chen, H.; Hu, J.; Wu, G.; Shi, W.; Geng, Y.; Qu, H. Apatite fission-track thermochronological constraints on the pattern of late Mesozoic–Cenozoic uplift and exhumation of the Qinling Orogen, central China. *J. Asian Earth Sci.* **2015**, *114*, 649–673. [CrossRef]
13. Liu, J.; Zhang, P.; Lease, R.O.; Zheng, D.; Wan, J.; Wang, W.; Zhang, H. Eocene onset and late Miocene acceleration of Cenozoic intracontinental extension in the North Qinling range–Weihe graben: Insights from apatite fission track thermo-chronology. *Tectonophysics* **2013**, *584*, 281–296. [CrossRef]
14. Lease, R.O.; Burbank, D.W.; Clark, M.K.; Farley, K.A.; Zheng, D.; Zhang, H. Middle Miocene reorganization of defor-mation along the northeastern Tibetan Plateau. *Geology* **2011**, *39*, 359–362. [CrossRef]
15. Wang, P.; Zheng, H.; Liu, S.; Hoke, G. Late Cretaceous drainage reorganization of the middle Yangtze River. *Lithosphere* **2018**, *10*, 392–405. [CrossRef]
16. Richardson, N.; Densmore, A.; Seward, D.; Wipf, M.; Yong, L. Did incision of the Three Gorges begin in the Eocene? *Geology* **2010**, *38*, 551–554. [CrossRef]
17. Yang, Z.; Shen, C.; Ratschbacher, L.; Enkelmann, E.; Jonckheere, R.; Wauschkuhn, B.; Dong, Y. Sichuan Basin and be-yond: Eastward foreland growth of the Tibetan Plateau from an integration of Late Cretaceous-Cenozoic fission track and (U-Th)/He ages of the eastern Tibetan Plateau, Qinling, and Daba Shan. *J. Geophys. Res. Solid Earth* **2017**, *122*, 4712–4740. [CrossRef]
18. Garver, J.I.; Brandon, M.T.; Roden-Tice, M.; Kamp, P.J.J. Exhumation history of orogenic highlands determined by detrital fission-track thermochronology. *Geol. Soc. London, Spéc. Publ.* **1999**, *154*, 283–304. [CrossRef]
19. Lin, X.; Jolivet, M.; Liu-Zeng, J.; Cheng, F.; Wu, Z.; Tian, Y.; Li, L.; Chen, J. The formation of the north qilian shan through time: Clues from detrital zircon fission-track data from modern river sediments. *Geosciences* **2022**, *12*, 166. [CrossRef]

20. Huyghe, P.; Bernet, M.; Galy, A.; Naylor, M.; Cruz, J.; Gyawali, B.; Gemignani, L.; Mugnier, J.-L. Rapid exhumation since at least 13 Ma in the Himalaya recorded by detrital apatite fission-track dating of Bengal fan (IODP Expedition 354) and modern Himalayan river sediments. *Earth Planet. Sci. Lett.* **2020**, *534*, 116078. [CrossRef]
21. Lin, X.; Jolivet, M.; Cheng, F. Spatiotemporal evolution of Central Qilian Shan (Northwest China) constrained by fis-sion-track ages of detrital grains from the Huangshui River. *Minerals* **2023**, *13*, 890. [CrossRef]
22. Bernet, M.; Brandon, M.T.; Garver, J.I.; Molitor, B.R.; Spiegel, C. Fundamentals of detrital zircon fission-track analysis for provenance and exhumation studies with examples from the European Alps. *Geol. Soc. Am. Spec. Publ.* **2004**, *378*, 25–36.
23. Bernet, M. Detrital zircon fission-track thermochronology of the present-day Isère River drainage system in the western alps: No evidence for increasing erosion rates at 5 Ma. *Geosciences* **2013**, *3*, 528–542. [CrossRef]
24. Malusà, M.G.; Zattin, M.; Andò, S.; Garzanti, E.; Vezzoli, G. Focused erosion in the Alps constrained by fission-track ages on detrital apatites. *Geol. Soc. London, Spéc. Publ.* **2009**, *324*, 141–152. [CrossRef]
25. Urueña-Suárez, C.L.; Peña-Urueña, M.L.; Muñoz-Rocha, J.A.; Rayo-Rocha, L.P.; Villamizar-Escalante, N.; Amaya-Ferreira, S.; Bernet, M. Zircon U–Pb and fission–track dating applied to resolving sediment provenance in modern rivers draining the Eastern and Central Cordilleras, Colombia. *Serv. Geol. Colomb. Publ. Geol. Espec* **2020**, *37*, 1–23.
26. Carrapa, B.; Mustapha, F.S.; Cosca, M.; Gehrels, G.; Schoenbohm, L.M.; Sobel, E.R.; DeCelles, P.G.; Russell, J.; Goodman, P. Multisystem dating of modern river detritus from Tajikistan and China: Implications for crustal evolution and exhumation of the Pamir. *Lithosphere* **2014**, *6*, 443–455. [CrossRef]
27. Li, L.; Najman, Y.; Dupont-Nivet, G.; Parra, M.; Roperch, P.; Kaya, M.; Aminov, J. Mesozoic–Cenozoic multistage tec-tonic evolution of the Pamir: Detrital fission-track constraints from the Tajik Basin. *Basin Res.* **2023**, *35*, 530–550. [CrossRef]
28. You, J.; Yang, Z.; Shi, X.; Shen, C.; Dong, Y.; Cheng, B. Exhumation and deformation of the Daba Shan Orocline as determined from modern river sands apatite fission-track. *J. Earth Sci.* **2023**, *34*, 1140–1149. [CrossRef]
29. Dong, Y.; Zhang, G.; Neubauer, F.; Liu, X.; Genser, J.; Hauzenberger, C. Tectonic evolution of the Qinling orogen, China: Review and synthesis. *J. Asian Earth Sci.* **2011**, *41*, 213–237. [CrossRef]
30. Li, J.; Zhang, Y.; Dong, S.; Shi, W. Structural and geochronological constraints on the Mesozoic tectonic evolution of the North Dabashan zone, South Qinling, central China. *J. Asian Earth Sci.* **2013**, *64*, 99–114. [CrossRef]
31. Meng, Q.-R.; Zhang, G.-W. Geologic framework and tectonic evolution of the Qinling orogen, central China. *Tectonophysics* **2000**, *323*, 183–196. [CrossRef]
32. Enkin, R.J.; Yang, Z.; Chen, Y.; Courtillot, V. Paleomagnetic constraints on the geodynamic history of the major blocks of China from the Permian to the present. *J. Geophys. Res. Solid Earth* **1992**, *97*, 13953–13989. [CrossRef]
33. Dong, S.; Zhang, Y.; Long, C.; Yang, Z.; Ji, Q.; Wang, T.; Hu, J.; Chen, X. Jurassic tectonic revolution in China and new interpretation of the "Yanshan Movement". *Acta Geol. Sin. Engl. Ed.* **2008**, *82*, 334–347.
34. Song, P.; Teng, J.; Zhang, X.; Liu, Y.; Si, X.; Ma, X.; Qiao, Y.; Dong, X. Flyover crustal structures beneath the Qinling Orogenic Belt and its tectonic implications. *J. Geophys. Res. Solid Earth* **2018**, *123*, 6703–6718. [CrossRef]
35. Li, S.; Guo, L.; Xu, L.; Somerville, I.D.; Cao, X.; Yu, S.; Wang, P.; Suo, Y.; Liu, X.; Zhao, S. Coupling and transition of Meso–Cenozoic intracontinental deformation between the Taihang and Qinling Mountains. *J. Asian Earth Sci.* **2015**, *114*, 188–202. [CrossRef]
36. Shi, X.; Yang, Z.; Dong, Y.; Qu, H.; Zhou, B.; Cheng, B. Geomorphic indices and longitudinal profile of the Daba Shan, northeastern Sichuan Basin: Evidence for the late Cenozoic eastward growth of the Tibetan Plateau. *Geomorphology* **2020**, *353*, 107031. [CrossRef]
37. Einsele, G. *Sedimentary Basins: Evolution, Facies, and Sediment Budget*; Springer: Berlin/Heidelberg, Germany, 2020; pp. 1–781.
38. Zhai, M.; Santosh, M. Metallogeny of the North China Craton: Link with secular changes in the evolving Earth. *Gondwana Res.* **2013**, *24*, 275–297. [CrossRef]
39. Luo, L.; Qi, J.-F.; Zhang, M.-Z.; Wang, K.; Han, Y.-Z. Detrital zircon U–Pb ages of Late Triassic–Late Jurassic deposits in the western and northern Sichuan Basin margin: Constraints on the foreland basin provenance and tectonic implications. *Int. J. Earth Sci.* **2014**, *103*, 1553–1568. [CrossRef]
40. Shi, W.; Dong, S.-W.; Ratschbacher, L.; Tian, M.; Li, J.-H.; Wu, G.-L. Meso-Cenozoic tectonic evolution of the Dangyang Basin, north-central Yangtze craton, central China. *Int. Geol. Rev.* **2013**, *55*, 382–396. [CrossRef]
41. Xu, Y.; He, D. Triassic provenance shifts and tectonic evolution of southeast Ordos Basin, Central China. *Palaeogeogr. Palaeoclim. Palaeoecol.* **2022**, *598*, 111002. [CrossRef]
42. Li, Z.C.; Li, W.H.; Li, Y.X.; Li, Y.H.; Han, W. Cenozoic stratigraphy and Paleoenvironments in the Weihe area, Shaanxi province. *Stratigraphy* **2016**, *40*, 168–179.
43. Liu-Zeng, J.; Tapponnier, P.; Gaudemer, Y.; Ding, L. Quantifying landscape differences across the Tibetan plateau: Im-plications for topographic relief evolution. *J. Geophys. Res. Earth Surf.* **2008**, *113*, 1–26. [CrossRef]
44. Clark, M.K.; Schoenbohm, L.M.; Royden, L.H.; Whipple, K.X.; Burchfiel, B.C.; Zhang, X.; Tang, W.; Wang, E.; Chen, L. Surface uplift, tectonics, and erosion of eastern Tibet from large-scale drainage patterns. *Tectonics* **2004**, *23*, 1–21. [CrossRef]
45. Brookfield, M. The evolution of the great river systems of southern Asia during the Cenozoic India-Asia collision: Rivers draining southwards. *Geomorphology* **1998**, *22*, 285–312. [CrossRef]
46. Xie, W.; Wang, X.; Zhang, H.; Liu, Q.; Wang, S.; Lu, H. Drainage evolution in intermontane basins at the Qinling-Daba Mountains. *Sci. China Earth Sci.* **2021**, *64*, 1949–1968. [CrossRef]

47. Clift, P.D.; Van Long, H.; Hinton, R.; Ellam, R.M.; Hannigan, R.; Tan, M.T.; Blusztajn, J.; Duc, N.A. Evolving east Asian river systems reconstructed by trace element and Pb and Nd isotope variations in modern and ancient Red River-Song Hong sediments. *Geochem. Geophys. Geosyst.* **2008**, *9*, 1–29. [CrossRef]
48. Zheng, H.; Clift, P.D.; He, M.; Bian, Z.; Liu, G.; Liu, X.; Xia, L.; Yang, Q.; Jourdan, F. Formation of the First Bend in the late Eocene gave birth to the modern Yangtze River, China. *Geology* **2021**, *49*, 35–39. [CrossRef]
49. Yan, Y.; Yao, D.; Tian, Z.; Huang, C.; Dilek, Y.; Clift, P.D.; Li, Z. Tectonic topography changes in cenozoic east asia: A landscape erosion-sediment archive in the South China Sea. *Geochem. Geophys. Geosyst.* **2018**, *19*, 1731–1750. [CrossRef]
50. Fu, X.; Zhu, W.; Geng, J.; Yang, S.; Zhong, K.; Huang, X.; Zhang, L.; Xu, X. The present-day Yangtze River was established in the late Miocene: Evidence from detrital zircon ages. *J. Asian Earth Sci.* **2021**, *205*, 104600. [CrossRef]
51. Shen, X.; Tian, Y.; Li, D.; Qin, S.; Vermeesch, P.; Schwanethal, J. Oligocene-Early Miocene river incision near the first bend of the Yangze River: Insights from apatite (U-Th-Sm)/He thermochronology. *Tectonophysics* **2016**, *687*, 223–231. [CrossRef]
52. Su, H.; Dong, M.; Hu, Z. Late Miocene birth of the Middle Jinsha River revealed by the fluvial incision rate. *Glob. Planet. Chang.* **2019**, *183*, 103002. [CrossRef]
53. Zhang, D.; Cao, K.; Yuan, X.; Wang, G.; van der Beek, P. Late Oligocene-early Miocene Origin of the First Bend of the Yangtze River explained by thrusting-induced river reorganization. *Geomorphology* **2022**, *411*, 108303. [CrossRef]
54. Liu, Y. Neogene fluvial sediments in the northern Jinshaan Gorge, China: Implications for early development of the Yellow River since 8 Ma and its response to rapid subsidence of the Weihe-Shanxi Graben. *Palaeogeogr. Palaeoclim. Palaeoecol.* **2020**, *546*, 109675. [CrossRef]
55. Bao, G.; Chen, H.; Zhao, X. Late Miocene Yellow River formation in Qingtongxia area, North China: Detrital zircon and heavy mineral analysis at Niushou Mountain, Ningxia. *Geol. J.* **2020**, *55*, 7304–7321. [CrossRef]
56. Lu, H.; Wang, X.; An, Z.; Miao, X.; Zhu, R.; Ma, H.; Wang, X. Geomorphologic evidence of phased uplift of the north-eastern Qinghai-Tibet Plateau since 14 million years ago. *Sci. China Ser. D Earth Sci.* **2004**, *47*, 822–833. [CrossRef]
57. Kong, P.; Jia, J.; Zheng, Y. Time constraints for the Yellow River traversing the Sanmen Gorge. *Geochem. Geophys. Geosyst.* **2014**, *15*, 395–407. [CrossRef]
58. Yang, J.; Yuan, H.; Hu, Y.; Wang, F. Significance of sedimentary provenance reconstruction based on borehole records of the North China Plain for the evolution of the Yellow River. *Geomorphology* **2022**, *401*, 108077. [CrossRef]
59. Sobel, E.; Seward, D. Influence of etching conditions on apatite fission-track etch pit diameter. *Chem. Geol.* **2010**, *271*, 59–69. [CrossRef]
60. Hasebe, N.; Barbarand, J.; Jarvis, K.; Carter, A.; Hurford, A.J. Apatite fission-track chronometry using laser ablation ICP-MS. *Chem. Geol.* **2004**, *207*, 135–145. [CrossRef]
61. Soares, C.J.; Guedes, S.; Hadler, J.C.; Mertz-Kraus, R.; Zack, T.; Iunes, P.J. Novel calibration for LA-ICP-MS-based fis-sion-track thermochronology. *Phys. Chem. Miner.* **2014**, *41*, 65–73. [CrossRef]
62. Hurford, A.J.; Green, P.F. The zeta age calibration of fission-track dating. *Chem. Geol.* **1983**, *41*, 285–317. [CrossRef]
63. McDowell, F.A.; McIntosh, W.C.; Farley, K. A precise 40Ar–39Ar reference age for the Durango apatite (U–Th)/He and fission-track dating standard. *Chem. Geol.* **2005**, *214*, 249–263. [CrossRef]
64. Vermeesch, P. On the visualisation of detrital age distributions. *Chem. Geol.* **2012**, *312–313*, 190–194. [CrossRef]
65. Yin, A.; Nie, S. An indentation model for the North and South China collision and the development of the Tan-Lu and Honam Fault Systems, eastern Asia. *Tectonics* **1993**, *12*, 801–813. [CrossRef]
66. Lu, G.; Li, C.; Li, W.; Deng, S.; Zhang, J. Structural geometry and kinematics of thrust belts between the Dabashan and eastern Sichuan Basin, South China block: Constraints from (U-Th)/He dating and seismic data. *GSA Bull.* **2021**, *133*, 1749–1764. [CrossRef]
67. Wu, C.; Zuza, A.V.; Levy, D.A.; Li, J.; Ding, L. Discovery of Permian–Triassic eclogite in northern Tibet establishes coeval subduction erosion along an ~3000-km-long arc. *Geology* **2023**, *51*, 833–838. [CrossRef]
68. Yang, Z.; Ratschbacher, L.; Jonckheere, R.; Enkelmann, E.; Dong, Y.; Shen, C.; Wiesinger, M.; Zhang, Q. Late-stage foreland growth of China's largest orogens (Qinling, Tibet): Evidence from the Hannan-Micang crystalline massifs and the northern Sichuan Basin, central China. *Lithosphere* **2013**, *5*, 420–437. [CrossRef]
69. Liu, S.; Heller, P.L.; Zhang, G. Mesozoic basin development and tectonic evolution of the Dabieshan orogenic belt, central China. *Tectonics* **2003**, *22*, 1–21. [CrossRef]
70. Li, Y.; He, D.; Li, D.; Lu, R.; Fan, C.; Sun, Y.; Huang, H. Sedimentary provenance constraints on the Jurassic to Cretaceous paleogeography of Sichuan Basin, SW China. *Gondwana Res.* **2018**, *60*, 15–33. [CrossRef]
71. Meng, L.; Chen, W.; Shen, T.; Cai, J. A Study on the provenance of Early to Late Triassic clastic rocks from the North-western Sichuan Basin, Southwestern China: Constraints on the early Mesozoic tectonic evolution of the western Yangtze Block. *Front. Earth Sci.* **2022**, *10*, 940301. [CrossRef]
72. Cao, Z.; Deng, B.; Hu, X.; Yang, R.; Xu, H.; Liu, C.; Qiu, Y.; Zheng, C.; Liu, G.; Liu, S. Tectonic chronology and sedimentary response characteristics of the late Triassic source sink system in the northwestern margin of Sichuan. *Nat. Gas Geosci.* **2023**, *10*, 1–20. (In Chinese with English Abstract)
73. Xie, X. Provenance and sediment dispersal of the Triassic Yanchang Formation, southwest Ordos Basin, China, and its implications. *Sediment. Geol.* **2016**, *335*, 1–16. [CrossRef]

74. Yu, Q.; Ren, Z.; Li, R.; Ling, C.; Ni, T.; Lei, W.; Wang, B.; Wu, X.; Qin, X.; Lei, X. Different burial-cooling history of Triassic strata between the western Weibei Uplift and the Northwestern Weihe Basin in Northwest China. *J. Earth Sci.* **2023**, 1–13. [CrossRef]
75. Yu, Q.; Ren, Z.; Li, R.; Chung, L.; Tao, N.; Cui, J.; Wang, B.; Qi, K.; Khaled, A. Cooling history of the southwestern Ordos Basin (northern China) since Late Jurassic: Insights from thermochronology and geothermometry. *J. Asian Earth Sci.* **2021**, *219*, 104895. [CrossRef]
76. Shen, C.; Hu, D.; Shao, C.; Mei, L. Thermochronology quantifying exhumation history of the Wudang Complex in the South Qinling Orogenic Belt, central China. *Geol. Mag.* **2018**, *155*, 893–906. [CrossRef]
77. Wang, M.; Tian, Y.; Zhou, B.; Jiao, R.; Zhang, G. Instant far-field effects of continental collision: An example study in the Qinling Orogen, northeast of the Tibetan Plateau. *Tectonophysics* **2022**, *833*, 229334. [CrossRef]
78. Reiners, P.W.; Zhou, Z.; Ehlers, T.A.; Xu, C.; Brandon, M.T.; Donelick, R.A.; Nicolescu, S. Post-orogenic evolution of the Dabie Shan, eastern China, from (U-Th)/He and fission-track thermochronology. *Am. J. Sci.* **2003**, *303*, 489–518. [CrossRef]
79. Shen, C.-B.; Mei, L.-F.; Xu, S.-H. Fission track dating of Mesozoic sandstones and its tectonic significance in the Eastern Sichuan Basin, China. *Radiat. Meas.* **2009**, *44*, 945–949. [CrossRef]
80. Tian, Y.; Qiu, N.; Kohn, B.P.; Zhu, C.; Hu, S.; Gleadow, A.J.; McInnes, B.I. Detrital zircon (U–Th)/He thermochronometry of the Mesozoic Daba Shan Foreland Basin, central China: Evidence for timing of post-orogenic denudation. *Tectonophysics* **2012**, *570*, 65–77. [CrossRef]
81. Peng, L.; Shen, C.; Yang, Z.; Ge, X. Apatite fission-track data from upper Cretaceous formations in the Yuan'an Graben (China): Constraints on the timing of synsedimentary fault activity. *Radiat. Meas.* **2013**, *50*, 187–191. [CrossRef]
82. Yang, F.; Jepson, G.; Liu, C.; Qian, Z.; Zhang, X.; Zhang, Y.; Glorie, S. Uplift-exhumation and preservation of the Yumugou Mo-W deposit, East Qinling, China: Insights from multiple apatite low-temperature thermochronology. *Ore Geol. Rev.* **2022**, *141*, 104670. [CrossRef]
83. Shen, C.; Mei, L.; Peng, L.; Chen, Y.; Yang, Z.; Hong, G. LA-ICPMS U–Pb zircon age constraints on the provenance of Cretaceous sediments in the Yichang area of the Jianghan Basin, central China. *Cretac. Res.* **2012**, *34*, 172–183. [CrossRef]
84. Chen, Y.; Li, J.; Miao, P.; Chen, L.; Zhao, H.; Wang, C. U-Pb ages and Hf isotopes of detrital zircons from the Cretaceous succession in the southwestern Ordos Basin, Northern China: Implications for provenance and tectonic evolution. *J. Asian Earth Sci.* **2021**, *219*, 104896. [CrossRef]
85. Li, J.; Zhang, Y.; Dong, S.; Johnston, S.T. Cretaceous tectonic evolution of South China: A preliminary synthesis. *Earth-Sci. Rev.* **2014**, *134*, 98–136. [CrossRef]
86. Dong, S.; Li, J.; Gao, R.; Cawood, P.A.; Thybo, H.; Johnston, S.T.; Jiao, L.; Zhang, Y.; Wang, J. Intraplate lithospheric extension revealed by seismic reflection profiling of South China. *Earth Planet. Sci. Lett.* **2023**, *609*, 118100. [CrossRef]
87. Li, J.; Dong, S.; Cawood, P.A.; Thybo, H.; Clift, P.D.; Johnston, S.T.; Zhao, G.; Zhang, Y. Cretaceous long-distance lithospheric extension and surface response in South China. *Earth-Sci. Rev.* **2023**, *243*, 104496. [CrossRef]
88. Clark, M.K.; Farley, K.A.; Zheng, D.; Wang, Z.; Duvall, A.R. 2010. Early Cenozoic faulting of the northern Tibetan Plateau margin from apatite (U–Th)/He ages. *Earth Planet. Sci. Lett.* **2010**, *296*, 78–88. [CrossRef]
89. He, P.; Wang, X.; Song, C.; Wang, Q.; Deng, L.; Zhong, S. Cenozoic evolution of the Western Qinling Mt. Range based on thermochronologic and sedimentary records from the Wudu Basin, NE Tibetan Plateau. *J. Asian Earth Sci.* **2017**, *138*, 484–494. [CrossRef]
90. Zhang, Y.-P.; Zheng, W.-J.; Wang, W.-T.; Tian, Y.-T.; Zhou, R.; Xu, B.-B.; Li, M.-J.; Yan, Y.-G.; Tian, Q.-Y.; Zhang, P.-Z. Rapid eocene exhumation of the West Qinling Belt: Implications for the growth of the Northeastern Tibetan Plateau. *Lithosphere* **2020**, *2020*, 8294751. [CrossRef]
91. Wang, X.; Zattin, M.; Li, J.; Song, C.; Peng, T.; Liu, S.; Liu, B. Eocene to Pliocene exhumation history of the Tianshui-Huicheng region determined by Apatite fission track thermochronology: Implications for evolution of the north-eastern Tibetan Plateau margin. *J. Asian Earth Sci.* **2011**, *42*, 97–110. [CrossRef]
92. Wang, W.; Zhang, P.; Liu, C.; Zheng, D.; Yu, J.; Zheng, W.; Chen, X. Pulsed growth of the West Qinling at ~30 Ma in northeastern Tibet: Evidence from Lanzhou Basin magnetostratigraphy and provenance. *J. Geophys. Res. Solid Earth* **2016**, *121*, 7754–7774. [CrossRef]
93. Ge, X.; Shen, C.; Yang, Z.; Mei, L.; Xu, S.; Peng, L.; Liu, Z. Low-temperature thermochronology constraints on the mes-ozoic-cenozoic exhumation of the Huangling massif in the Middle Yangtze Block, Central China. *J. Earth Sci.* **2013**, *24*, 541–552. [CrossRef]
94. Wu, L.; Mei, L.; Liu, Y.; Luo, J.; Min, C.; Lu, S.; Guo, L. Multiple provenance of rift sediments in the composite ba-sin-mountain system: Constraints from detrital zircon U-Pb geochronology and heavy minerals of the early Eocene Jianghan Basin, central China. *Sediment. Geol.* **2017**, *349*, 46–61. [CrossRef]
95. Yang, C.; Shen, C.; Zattin, M.; Yu, W. Formation of the Yangtze Three Gorges: Insights from detrital apatite fission-track dating of sediments from the Jianghan Basin. *Terra Nova* **2021**, *33*, 511–520. [CrossRef]
96. Chen, B.-L.; Yin, G.-M.; Li, W.-L.; Guo, L.; Li, L.; Lu, Y.-C.; Guo, S.-L. Determination of tectonic uplift rates of Qinling mountains in central China by fission tracks. *Radiat. Meas.* **2001**, *34*, 405–408. [CrossRef]
97. Lu, H.; Zhang, H.; Feng, H.; Wang, Y.; Cai, D.; Li, G.; Lyu, H.; Lei, F.; Wang, K.; Wang, S.; et al. Landform evolution in Asia during the Cenozoic revealed by formation of drainages of Wei River and Indus River. *Palaeogeogr. Palaeoclim. Palaeoecol.* **2023**, *619*, 111516. [CrossRef]

98. Wang, C.; Dai, J.; Zhao, X.; Li, Y.; Graham, S.A.; He, D.; Ran, B.; Meng, J. Outward-growth of the Tibetan Plateau during the Cenozoic: A review. *Tectonophysics* **2014**, *621*, 1–43. [CrossRef]
99. Ding, L.; Kapp, P.; Cai, F.; Garzione, C.N.; Xiong, Z.; Wang, H.; Wang, C. Timing and mechanisms of Tibetan Plateau uplift. *Nat. Rev. Earth Environ.* **2022**, *3*, 652–667. [CrossRef]
100. Deng, B.; Liu, S.-G.; Li, Z.-W.; Jansa, L.F.; Liu, S.; Wang, G.-Z.; Sun, W. Differential exhumation at eastern margin of the Tibetan Plateau, from apatite fission-track thermochronology. *Tectonophysics* **2013**, *591*, 98–115. [CrossRef]
101. Molnar, P.; England, P.; Martinod, J. Mantle dynamics, uplift of the Tibetan Plateau, and the Indian monsoon. *Rev. Geophys.* **1993**, *31*, 357–396. [CrossRef]
102. Jolivet, M.; Brunel, M.; Seward, D.; Xu, Z.; Yang, J.; Roger, F.; Tapponnier, P.; Malavieille, J.; Arnaud, N.; Wu, C. Mesozoic and Cenozoic tectonics of the northern edge of the Tibetan plateau: Fission-track constraints. *Tectonophysics* **2001**, *343*, 111–134. [CrossRef]
103. Tian, Y.; Li, R.; Tang, Y.; Xu, X.; Wang, Y.; Zhang, P. Thermochronological constraints on the late Cenozoic mor-photectonic evolution of the Min Shan, the eastern margin of the Tibetan Plateau. *Tectonics* **2018**, *37*, 1733–1749. [CrossRef]
104. Zheng, D.; Zhang, P.Z.; Wan, J.; Yuan, D.; Li, C.; Yin, G.; Chen, J. Rapid exhumation at ~8 Ma on the Liupan Shan thrust fault from apatite fission-track thermochronology: Implications for growth of the northeastern Tibetan Plateau margin. *Earth Planet. Sci. Lett.* **2006**, *248*, 198–208. [CrossRef]
105. Meng, Q.-R.; Wu, G.-L.; Fan, L.-G.; Wei, H.-H. Tectonic evolution of early Mesozoic sedimentary basins in the North China block. *Earth-Sci. Rev.* **2019**, *190*, 416–438. [CrossRef]
106. Dong, Y.; Santosh, M. Tectonic architecture and multiple orogeny of the Qinling Orogenic Belt, Central China. *Gondwana Res.* **2016**, *29*, 1–40. [CrossRef]
107. Liu, S.; Deng, B.; Jansa, L.; Li, Z.; Sun, W.; Wang, G.; Yong, Z. Multi-stage basin development and hydrocarbon accu-mulations: A review of the Sichuan Basin at eastern margin of the Tibetan Plateau. *J. Earth Sci.* **2018**, *29*, 307–325. [CrossRef]
108. Wu, L.; Mei, L.; Liu, Y.; Paton, D.A.; Luo, J.; Yu, L.; Wang, D.; Min, C.; Li, M.; Guo, L.; et al. The stratigraphic and structural record of the Cretaceous Jianghan Basin, central China: Implications for initial rifting processes and geodynamics. *Cretac. Res.* **2018**, *90*, 21–39. [CrossRef]
109. Su, J.C.; Lin, X.; Li, C.; Jolivet, M.; Wu, L.; Cheng, F.; Deng, B.; Wu, Z.; Chen, X.; Hu, C. Late Mesozoic exhumation of the Huangling Massif: Constraints on the evolution of the middle Yangtze River. *Acta Geol. Sin. Engl. Ed.* **2023**, *in press*. [CrossRef]
110. Deng, B.; Chew, D.; Jiang, L.; Mark, C.; Cogné, N.; Wang, Z.; Liu, S. Heavy mineral analysis and detrital U-Pb ages of the intracontinental Paleo-Yangzte basin: Implications for a transcontinental source-to-sink system during Late Cretaceous time. *GSA Bull.* **2018**, *130*, 2087–2109. [CrossRef]
111. Lin, X.; Liu-Zeng, J.; Jolivet, M.; Liu, W.; Cheng, F.; Liu, H.; Li, L.; Chen, J.; Hu, C.; Chen, X. Sedimentary provenance constraints on the Cretaceous to Cenozoic palaeogeography of the western margin of the Jianhan Basin, South China. *Gondwana Res.* **2023**, *125*, 343–358. [CrossRef]
112. Zhu, D.-C.; Zhao, Z.-D.; Niu, Y.; Mo, X.-X.; Chung, S.-L.; Hou, Z.-Q.; Wang, L.-Q.; Wu, F.-Y. The Lhasa Terrane: Record of a microcontinent and its histories of drift and growth. *Earth Planet. Sci. Lett.* **2011**, *301*, 241–255. [CrossRef]
113. Liu, D.L.; Shi, R.D.; Ding, L.; Zou, H.B. Late Cretaceous transition from subduction to collision along the Ban-gong-Nujiang Tethys: New volcanic constraints from central Tibet. *Lithos* **2018**, *296*, 452–470. [CrossRef]
114. Jolivet, M. Mesozoic tectonic and topographic evolution of Central Asia and Tibet: A preliminary synthesis. *Geol. Soc. Lond. Spéc. Publ.* **2017**, *427*, 19–55. [CrossRef]
115. Liu-Zeng, J.; Zhang, J.; McPhillips, D.; Reiners, P.; Wang, W.; Pik, R.; Zeng, L.; Hoke, G.; Xie, K.; Xiao, P.; et al. Multiple episodes of fast exhumation since Cretaceous in southeast Tibet, revealed by low-temperature thermochronology. *Earth Planet. Sci. Lett.* **2018**, *490*, 62–76. [CrossRef]
116. Dai, J.; Wang, C.; Hourigan, J.; Santosh, M. Multi-stage tectono-magmatic events of the Eastern Kunlun Range, northern Tibet: Insights from U–Pb geochronology and (U–Th)/He thermochronology. *Tectonophysics* **2013**, *599*, 97–106. [CrossRef]
117. Dai, J.; Wang, C.; Polat, A.; Santosh, M.; Li, Y.; Ge, Y. Rapid forearc spreading between 130 and 120Ma: Evidence from geochronology and geochemistry of the Xigaze ophiolite, southern Tibet. *Lithos* **2013**, *172*, 1–16. [CrossRef]
118. Wang, L.; Shen, L.; Liu, C.; Chen, K.; Ding, L.; Wang, C. The Late Cretaceous source-to-sink system at the eastern margin of the Tibetan Plateau: Insights from the provenance of the Lanping Basin. *Geosci. Front.* **2021**, *12*, 101102. [CrossRef]
119. Wang, L.; Ding, L.; Garzanti, E.; Shen, L.; Nulay, P.; Siritongkham, N. Mid-Cretaceous drainage reorganization and exorheic to endorheic transition in Southeast Tibet. *Sediment. Geol.* **2022**, *439*, 106221. [CrossRef]
120. Zhao, X.; Zhang, H.; Hetzel, R.; Kirby, E.; Duvall, A.R.; Whipple, K.X.; Xiong, J.; Li, Y.; Pang, J.; Wang, Y.; et al. Existence of a continental-scale river system in eastern Tibet during the late Cretaceous–early Palaeogene. *Nat. Commun.* **2021**, *12*, 7231. [CrossRef]
121. Wu, C.; Sun, X.; Li, G.; Huang, L.; Jiao, H.; Li, Z.; Jian, X.; Mason, C.C.; Rodríguez-López, J.P. Cretaceous mountain building processes triggered the aridification and drainage evolution in east Asia. *GSA Bull.* **2023**, *in press*. [CrossRef]
122. Li, S.; Currie, B.S.; Rowley, D.B.; Ingalls, M. Cenozoic paleoaltimetry of the SE margin of the Tibetan Plateau: Constraints on the tectonic evolution of the region. *Earth Planet. Sci. Lett.* **2015**, *432*, 415–424. [CrossRef]
123. Jiao, R.; Fox, M.; Yang, R. Late Cenozoic erosion pattern of the eastern margin of the Sichuan Basin: Implications for the drainage evolution of the Yangtze River. *Geomorphology* **2022**, *398*, 108025. [CrossRef]

124. Zhang, Y.Q.; Mercier, J.L.; Vergély, P. Extension in the graben systems around the Ordos (China), and its contribution to the extrusion tectonics of south China with respect to Gobi-Mongolia. *Tectonophysics* **1998**, *285*, 41–75. [CrossRef]
125. Shi, W.; Dong, S.; Hu, J. Neotectonics around the Ordos Block, North China: A review and new insights. *Earth-Sci. Rev.* **2020**, *200*, 102969. [CrossRef]
126. Lin, A.; Yang, Z.; Sun, Z.; Yang, T. How and when did the Yellow River develop its square bend? *Geology* **2001**, *29*, 951–954. [CrossRef]
127. Zheng, H.; Jia, D.; Chen, J.; Wang, P. Did incision of the Three Gorges begin in the Eocene? COMMENT. *Geology* **2011**, *39*, e244. [CrossRef]
128. Wu, L.; Wang, F.; Yang, J.; Wang, Y.; Zhang, W.; Yang, L.; Shi, W. Meso-Cenozoic uplift of the Taihang Mountains, North China: Evidence from zircon and apatite thermochronology. *Geol. Mag.* **2020**, *157*, 1097–1111. [CrossRef]
129. Huang, X.; Wang, Y.; Zhang, J.; Wu, F.; Yang, Y. Low-temperature thermochronological insights into the Mesozoic–Cenozoic exhumation history of the Taihang–Lvliangshan region: A review. *Geol. J.* **2022**, *57*, 1511–1529. [CrossRef]
130. Yu, J.; Zheng, D.; Pang, J.; Li, C.; Wang, Y.; Wang, Y.; Hao, Y.; Zhang, P. Cenozoic mountain building in eastern China and its correlation with reorganization of the Asian climate regime. *Geology* **2022**, *50*, 859–863. [CrossRef]
131. Nie, J.; Peng, W.; Möller, A.; Song, Y.; Stockli, D.F.; Stevens, T.; Horton, B.K.; Liu, S.; Bird, A.; Oalmann, J.; et al. Provenance of the upper Miocene–Pliocene Red Clay deposits of the Chinese loess plateau. *Earth Planet. Sci. Lett.* **2014**, *407*, 35–47. [CrossRef]
132. Sun, J.; Ding, Z.; Xiao, W.; Windley, B.F. Coupling between uplift of the Central Asian Orogenic Belt-NE Tibetan Plateau and accumulation of aeolian Red Clay in the inner Asia began at ~7 Ma. *Earth Sci. Rev.* **2022**, *226*, 103919. [CrossRef]
133. Deng, B.; Chew, D.; Mark, C.; Liu, S.; Cogné, N.; Jiang, L.; O'sullivan, G.; Li, Z.; Li, J. Late Cenozoic drainage reorganization of the paleo-Yangtze river constrained by multi-proxy provenance analysis of the Paleo-lake Xigeda. *GSA Bull.* **2021**, *133*, 199–211. [CrossRef]
134. Zhao, X.; Zhang, H.; Tao, Y.; Wang, Y.; Pang, J.; Ma, Y.; Zhang, J.; Ma, Z.; Xiong, J. Pliocene to Early Pleistocene Drainage Reorganization in Eastern Tibet Inferred From Detrital Zircons. *Geophys. Res. Lett.* **2021**, *48*, e2021GL094563. [CrossRef]
135. Liu, D.; Li, H.; Wang, P.; Pan, J.; Zheng, Y.; Zhu, X. Sedimental provenance response in the northern South China Sea to the Cenozoic fluvial evolution. *Acta Geol. Sin.* **2022**, *96*, 2761–2774. (In Chinese with English Abstract)
136. McPhillips, D.; Hoke, G.D.; Liu-Zeng, J.; Bierman, P.R.; Rood, D.H.; Niedermann, S. Dating the incision of the Yangtze River gorge at the First Bend using three-nuclide burial ages. *Geophys. Res. Lett.* **2016**, *43*, 101–110. [CrossRef]
137. Yang, C.; Shen, C.; Zattin, M.; Yu, W.; Shi, S.; Mei, L. Provenances of Cenozoic sediments in the Jianghan Basin and implications for the formation of the Three Gorges. *Int. Geol. Rev.* **2019**, *61*, 1980–1999. [CrossRef]